coatings

MDPI

Article

Thymol-Functionalized Silica Nanomaterials Prepared by Post-Grafting Method: Preparation, Characterization, Bactericidal Activity and Mechanism Research

Liang Wang [1], Tianjun Ni [2,*] and Shiqin Wei [3,*]

[1] School of Food Science and Technology, Jiangnan University, Wuxi 214122, China
[2] School of Basic Medicine, Xinxiang Medical University, Xinxiang 453003, China
[3] School of Materials Science and Engineering, University of New South Wales (UNSW), Sydney, NSW 2052, Australia
* Correspondence: tjni@xxmu.edu.cn (T.N.); shiqin.wei@student.unsw.edu.au (S.W.); Tel.: +86-135-0343-1774 (T.N.)

Abstract: In this study, thymol was covalently connected to mesoporous silica nanomaterial by a post-grafting method to obtain a stable antibacterial system, thus overcoming the volatilization of thymol, prolonging the effective time of antibacterial action, and enhancing the antibacterial efficiency of thymol. It was proposed for the first time that such a synthetic route be adopted to synthesize silica-based mesoporous/essential oil antibacterial materials. The post-grafting method could be capable of retaining the mesoporous original structure, which could effectively avoid the porosity reduction and disordered products caused by condensation. Among them, the minimum bactericidal concentration (MBC) of functionalized MCM-41 (silica support) for *E. coli* and *S. aureus* were 0.3 mg mL^{-1} and 0.4 mg mL^{-1}, which were equivalent to 3/4 and 4/5 of free thymol (0.4 mg mL^{-1} and 0.5 mg mL^{-1}), respectively. Meanwhile, the MBC of functionalized SBA-15 (silica support) for *E. coli* and *S. aureus* were both 0.2 mg mL^{-1}, which also reduced the MBC of free thymol. These results revealed thymol-functionalized mesoporous silica nanomaterial could efficiently improve the bactericidal activities of the organic component. Finally, the inhibition mechanism of the post-grafting strategy was also discussed, which referred to how the antibacterial material directly acts on the cell membrane, resulting in cell inactivation.

Keywords: thymol; nano mesoporous materials; post-grafting method; antimicrobial activity

Citation: Wang, L.; Ni, T.; Wei, S. Thymol-Functionalized Silica Nanomaterials Prepared by Post-Grafting Method: Preparation, Characterization, Bactericidal Activity and Mechanism Research. *Coatings* **2023**, *13*, 86. https://doi.org/10.3390/coatings13010086

Academic Editor: Seunghan Oh

Received: 6 November 2022
Revised: 26 November 2022
Accepted: 1 December 2022
Published: 3 January 2023

1. Introduction

Antibacterial agents are compounds that can kill bacterial cells or inhibit their growth. Hence, they are increasingly seen as important to human health. Bacteriostat includes a variety of substances, including pure natural substances, chemically modified natural substances, and completely chemically synthesized compounds. However, given antibiotic resistance, new strategies which can propose additional agents with innovative action are urgently needed [1].

At the same time, more and more foodborne diseases have made public health problems more serious, which have aroused wide public concern about the health and environmental safety of chemical synthesis compounds [2–4]. Therefore, pure organic substances instead of chemically synthesized substances will be favored by consumers [5]. In this case, the development of novel antibacterial compounds with long-term effects was deemed to be an urgent and basic need of the food industry [6,7].

Essential oils are concentrated natural products with a strong odor produced by aromatic plants, which can protect plants from a variety of pathogenic microorganisms [8,9]. At the same time, it is generally believed that essential oils have antibacterial, antifungal, antiviral, and antioxidant properties that can replace chemically synthesized antibacterial

agents and serve as natural additives for food [10]. The significant antibacterial activity of essential oils can be attributed to the interaction of phenolic compounds with microbial cell membranes, leading to cytoplasmic outflow and ultimately cell destruction [11]. Although essential oils have broad application prospects as food-borne microbial antibacterial agents in the food industry, their shortcomings, such as high volatility, strong odor, poor water solubility, and poor stability, greatly limit their industrial applications [12,13]. So, there is an urgent need to find a new strategy to eliminate the negative effects of essential oils while maintaining or enhancing the antibacterial activity of essential oils. One potential method is to immobilize essential oils on the surface of active molecules [14,15].

Among potential immobilized carriers, nanomaterials exhibit unique advantages. Due to the high surface-to-volume ratio, nanomaterials increase the contact area with microorganisms, thus enhancing the antibacterial activity [16]. In particular, mesoporous silica nanoparticles have received more and more attention in recent years. Mesoporous silica nanoparticles have the advantages of high specific surface area, adjustable pore size and particle size, controllable morphology, high mechanical or thermal stability, and selective functionalization of internal and external surfaces [17]. These advantages make it easier to design drug delivery systems based on nanoparticles [11,18].

Here, two kinds of mesoporous silica carriers (MCM-41 and SBA-15) were selected. Thus, we obtained a long-acting and efficient thymol mesoporous silica nanomaterial antibacterial carrier because thymol was fixed on these two mesoporous silica carriers by a post-grafting method [19]. The key purpose of this paper is to improve the stability of thymol to the maximum extent and increase the utilization rate of raw materials by preparing a stable and efficient antibacterial system, making it more suitable for industrial production. The structural characteristics and the degree of functionalization of the prepared antibacterial carriers were explored by characterizing them in the course of our experiments. At the same time, the antibacterial activities of the prepared antibacterial carrier against food-borne pathogenic bacteria (*E. coli* and *S. aureus*) were studied.

2. Materials and Methods

2.1. Experimental Materials and Reagents

Shanghai Shenggong Biological Co., LTD (Shanghai, China) provided 2-isopropyl-5-methylphenol (thymol, 98%), tetraethyl orthosilicate (TEOS, 98%), aqueous ammonia (28%), cetyltrimethyl ammonium bromide (CTAB, 99%), POLYETHYLENE oxide-polypropylene oxide-polyethylene oxide (P123, 99%), anhydrous ethanol (99.8%), dimethyl sulfoxide (DMSO, 99%), sodium chloride (NaCl, 99%), and microbial culture medium. We purchased 3-(triethoxysilyl)-propyl-isocyanate (TEPIC, 95%), acetonitrile (99%), and tetrahydrofuran (THF, 99%) from Aladdin Biochemical Technology Co., Ltd. (Shanghai, China).

2.2. Preparation of Functionalized Mesoporous Silica by Grafting Method

Functional mesoporous silica was modified by grafting thymol onto the surface of mesoporous silica. The preparation and functionalization procedure was completed in three steps, each separately described in the following. The first basic part was the preparation of MCM-41 and SBA-15 mesoporous silica nanoparticles. Then, thymol silane derivatives were synthesized from thymol and TEPIC. Finally, mesoporous nanoparticles reacted with thymol silane derivatives to collect antibacterial carries. The main preparation and experimental process are shown in Figure 1.

2.2.1. Synthesis of Mesoporous Silicon

The MCM-41 was modified according to the literature, and the method was as follows [15,20]. To completely dissolve CTAB, 140 mL of aqueous ammonia and 2 g of CTAB were added to 200ml of deionized water and stirred for 1 h at 60 °C at 250 rpm. Then 7.5 g of TEOS was added dropwise and stirred for 6 h. After hydrolysis, the resulting white suspension crystallized at 33 °C for 24 h. Finally, the white suspension was filtered, washed, and dried at room temperature to obtain the solid white powder. In addition, the white

solid powder was calcined at 550 °C for 6h in a muffle furnace to remove the template to obtain MCM-41.

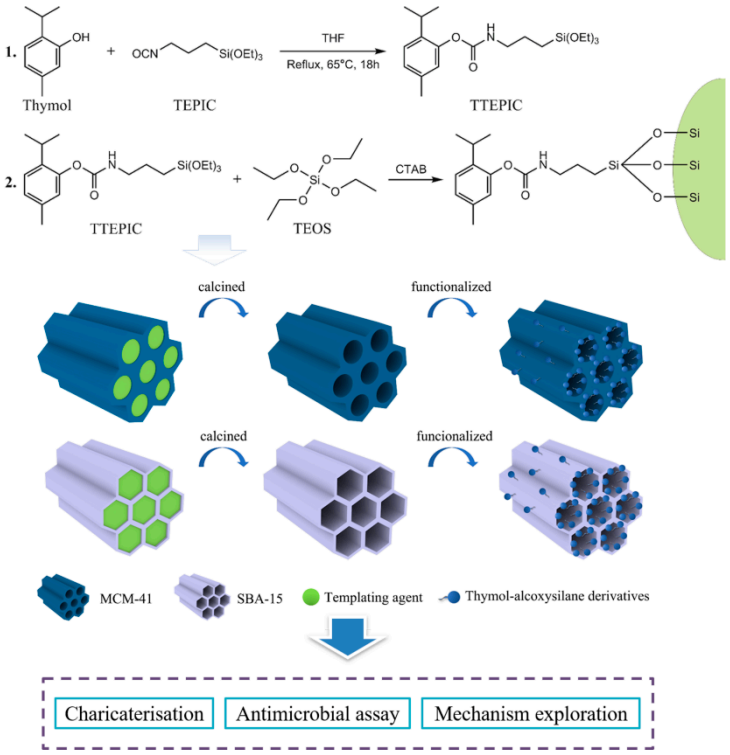

Figure 1. Preparation of functionalized mesoporous silica.

SBA-15 was synthesized in accordance with the literature, which is as follows: P123 was used as the template, and the molar ratio of reactant was 0.017 p123:1.0 TEOS:6 HCl:196 H_2O [21]. Firstly, the P123 template was dissolved in water and mixed with hydrochloric acid, stirring at 35 °C for 2 h. Secondly, it was hydrolyzed with TEOS from a silicon source and continued stirring at the same temperature for 20 h. After hydrolysis was completed, the crystals were enclosed in a constant temperature oven at 80 °C for 12 h. In addition, the mixture was filtered, washed, and dried at room temperature. The template had to be removed from the resulting white solid after 6 h at 550 °C.

2.2.2. Synthesis of Thymol Silane Derivatives

First, thymol was dissolved in a small amount of THF. After dissolving completely, TEPIC was added dropwise to the solution. The molar ratio of thymol to TEPIC was 1:1. The mixture was heated and stirred under a nitrogen atmosphere at 65 °C for about 18 h. The mixture was concentrated in a rotary vacuum evaporator at room temperature to remove the solvent THF until a transparent oily liquid was obtained.

2.2.3. Synthesis of Functionalized Mesoporous Silicon

According to the method reported in the literature, thymol functionalized mesoporous silica (Thy-MCM-41, Thy-SBA-15) was achieved through the following several procedures [22,23]. A white suspension was obtained after 1g of mesoporous silica (SBA-15 or MCM-41) was added to 40 mL of acetonitrile and stirred until uniformly dispersed. The thymol silane derivative was dropped into the white suspension, and stirring continued for 5.5 h at room temperature under a nitrogen atmosphere. The outcome was filtrated into a white solid, which was washed with acetonitrile and deionized water later. Finally, the product was put into a vacuum drying oven and dried at room temperature for 22 h to obtain Thy-MCM-41 and Thy-SBA-15.

2.3. Characterization

Standard techniques were used to examine the MCM-41, SBA-15, Thy-MCM-41, and Thy-SBA-15, including field emission scanning electron microscopy (FESEM), transmission electron microscopy (TEM), Fourier transform infrared spectroscopy (FT-IR), thermogravimetric analysis (TGA), N_2 adsorption/desorption isotherms, and small-angle X-ray diffraction (XRD).

In order to explore the physicochemical properties of Thy-MCM-41, Thy-SBA-15, MCM-41, and SBA-15, standard techniques were used. Figures of silica morphology were obtained by FESEM (Hitachi SU5000, Hitachi, Tokyo, Japan) at 6 kV acceleration voltages. The pore structures of MCM-41, SBA-15, Thy-MCM-41, and Thy-SBA-15 were observed by TEM (JEM-2100F, JEOL, Tokyo, Japan). The chemical composition of silica carriers was analyzed by FT-IR (Nicolet Instrument, Thermo Company, Waltham, MA, USA). Thermal stability analysis of silica particles was performed using a TGA (STA 409, Netzsch, Selb, Germany) at a heating rate of 10 K min^{-1} in an air-filled condition (80 mL min^{-1}) at a temperature of 30 to 800 °C. The N_2 adsorption and desorption isotherms were calculated by an automatic adsorption analyzer (ASAP 2460, Micromeritics, Norcross, GA, USA). The synthesis process and structure of mesoporous silica particles were analyzed by small-angle XRD (AXS D8 X-ray diffractometer, Bruker, Billerica, MA, USA). Copper Kα was elected as the radiation source. The operating current was 40 mA, and the voltage was 40 kV. The 2θ range was 10°–1.2°, and the scanning was performed at a rate of 1° min^{-1} and a step length of 0.01°.

2.4. Antibacterial Activity Assays

2.4.1. Culture Conditions and Bacterial Strain

Two strains, *E. coli* (Gram-negative) and *S. aureus* (Gram-positive), were obtained from Shanghai Ocean University. All strains were activated at −80 °C refrigerator for storage, then transferred to trypsin soybean AGAR (TSA) and stored in a 4 °C refrigerator for later use. A colony cell was picked up from the solid medium when needed and transferred to 10 mL of trypsin soybean broth (TSB). It was cultured at 37 °C for 24 h to obtain an inoculum density of about 10^8 CFU mL^{-1} for subsequent experiments.

2.4.2. Antibacterial Activity Assays In Vitro

The thymol on *E. coli* (ATCC8739NA) and *S. aureus* (ATCC12600) antibacterial activity based on the minimum bactericidal concentration (MBC) was determined by the microporous dilution method [24]. Different amounts of thymol were individually dissolved in 5% DMSO. Then, 100 μL of TSB solution was added to each well of the 96-well plate, and 100 μL of the prepared thymol solution was absorbed into the first well after repeated blowing and mixing. Subsequently, serial double dilutions were performed to obtain final concentrations ranging from 0.002 to 4 mg mL^{-1}. Finally, 10 μL diluted microbial suspension (about 1×10^7 CFU mL^{-1}) was added to each well to provide an initial bacteria density of approximately 10^6 CFU mL^{-1}. The 96-well plate was placed in a constant temperature incubator and incubated at 37 °C for 24 h. After incubation, MBC was determined by re-inoculating the medium diluted in the 96-well plate on solid medium. Colony formation units were counted and expressed as Log10 CFU mL^{-1} after incubation at 37 °C for 24 h by the continuous dilution coating method. All the treatments were performed in triplicate.

The antibacterial activities of thymol-functionalized antibacterial carriers (MCM-41 and SBA-15) against *E. coli* and *S. aureus* were studied by MBC. Firstly, two kinds of functionalized mesoporous silicon were put into 10 mL of TSB culture solution, respectively, and fully mixed by shock. Moreover, concentrations of suspension were dependent on the additive amount. The mass of functionalized particles, required by suspensions of different concentrations, was calculated by the result of TGA. Then, 100 μL microbial suspension was inoculated to make the initial cell density of 10^6 CFU mL^{-1}. Finally, the tube was placed in a shaker and incubated at 37 °C for 24 h at a speed of 150 rpm. The number of cultivable cells was determined by the continuous dilution coating method and incubated

at 37 °C for 24 h. The logarithm of the number of cultivable living cells was converted to Log10 CFU mL^{-1}. All experiments were repeated three times, including positive controls (tubes containing inoculants and nutrient solution) and negative controls (tubes containing functionalized mesoporous silicon and nutrient solution).

The percentage of cell growth reduction (R, %) was calculated using the following equation:

$$R = (C_0 - C)/C_0 \times 100\%$$

where C_0 is the number of CFU from the control sample, and C is the number of CFU from treated samples.

2.5. Sterilization Mechanism

In order to further explore the antibacterial mechanism of the carrier, the morphological changes of the two kinds of cells, SBA-15 and Thy-SBA-15 treatment, were observed by scanning electron microscopy. The specific operational steps were as follows. Different concentrations of SBA-15 antibacterial carriers were added into the suspension of *E. coli* and *S. aureus* that had been cultured for 24 h and incubated in a constant temperature incubator at 37 °C for 24 h. Subsequently, after samples were centrifuged at 4000 rpm speed for 10 min, the supernatant was discarded. Next, the bacterial solution was fixed using 2.5% glutaraldehyde. Then, the sample was washed with 0.1 M PSB buffer. The samples were dehydrated in ethanol solutions of different concentration gradient (30%, 50%, 70%, 90%, 100%). Dehydrated cells were freeze-dried in a freeze-dryer for 24 h, and the morphological changes of cells were observed under SEM.

2.6. Data Processing

Origin 9.0 software was used to make diagrams, and SPSS 20.0 software was used (Version 20.0; SPSS Inc., Chicago, IL, USA) to perform a one-way ANOVA on the data, and $p < 0.05$ was considered significant.

3. Results and Analysis

3.1. Material Characterization

Figure 2 depicts field emission scanning electron microscopy (FESEM) and transmission electron microscopic (TEM) images of MCM-41, SBA-15, Thy-MCM-41, and Thy-SBA-15. SEM and TEM images of both materials displayed superb morphologies and unitive particle size distributions in MCM-41 and SBA-15. Through FESEM results, it was found that MCM-41 presented a unique hexagonal prism morphology, with a particle size of about 4 μm, while SBA-15 posted a slender particle morphology, with a particle size of about 1.7 μm [25]. Furthermore, the surface roughness of modified mesoporous silica increased inconspicuously, which confirmed the immobilization process almost did not transform the completeness of the mesoporous silica particles and always maintained the unique morphology of different mesoporous silica particles. In the end, TEM images depicted the pore structure of two mesoporous silica nanoparticles. It could be observed that they all had the typical pore characteristics of mesoporous materials, that is, the black and white strip-shaped pores or the pores were arranged in a pseudo-hexagonal arrangement. These typical pore structures could be observed not only in the initial silica particles but also in the Thy-MCM-41 and Thy-SBA-15, demonstrating that the thymol-modified mesoporous materials retained the same structure.

Figure 3 depicts the FT-IR spectra of mesoporous silicon nanoparticles (a) MCM-41, (b) Thy-MCM-41, (c) SBA-15, and (d) Thy-SBA-15. All the FT-IR illustrate three characteristic peaks typical of silicon-oxygen tetrahedral. The broadband absorption peak at 1000-1300 cm^{-1} was explained by the antisymmetric stretching vibration of the Si–O tetrahedron [26]. The absorption near 790 cm^{-1} was attributed to the symmetric stretching vibration of the Si–OH tetrahedron [12]. The absorption peak around 445 cm^{-1} was because of the bending vibration of Si–O [27]. Furthermore, the absorption peak of functionalized mesoporous silica between 1600–1400 cm^{-1} might be the result of C=C stretching in the

benzene ring of thymol [28,29]. The wide peak at 3000–3600 cm^{-1} might be related to N–H and O–H vibration of adsorbed water in the coupling agent [30]. These results revealed that thymol was successfully bound on the surface of mesoporous silica particles".

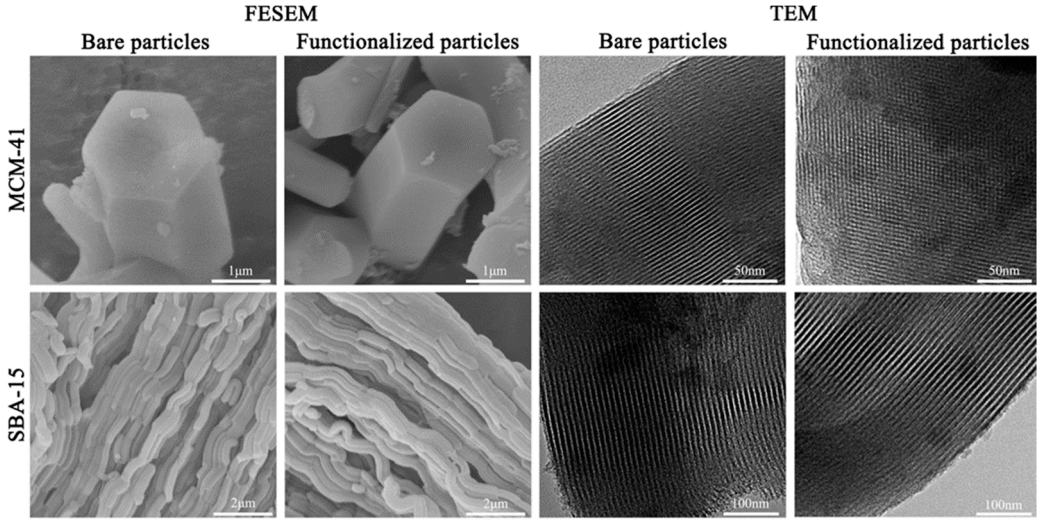

Figure 2. FESEM and TEM images of MCM-41, SBA-15, Thy-MCM-41, and Thy-SBA-15.

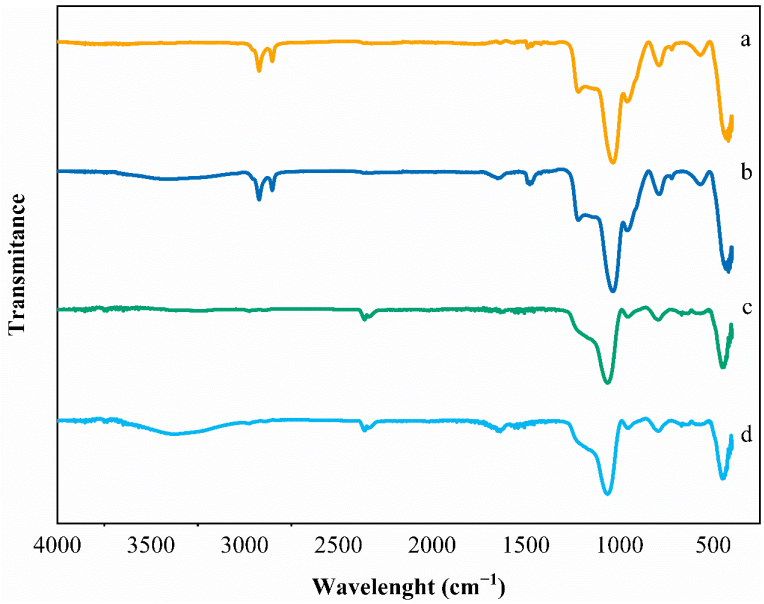

Figure 3. FT-IR of mesoporous silicon nanoparticles: (a) MCM-41; (b) Thy-MCM-41; (c) SBA-15; and (d) Thy-SBA-15.

Figure 4 shows the TGA curves of mesoporous silica nanoparticles mesoporous silicon nanoparticles MCM-41, SBA-15, Thy-MCM-41, and Thy-SBA-15. Both unmodified MCM-41 and SBA-15 exhibited a one-step weight loss in the range of 30–180 °C, which could be attributed to the loss of absorbed water molecules and used solvent in the synthesis. The weight loss process of Thy-MCM-41 and Thy-SBA-15 mainly divided into two stages. First, there was a slight weight loss before 180 °C, for the same reason as unmodified particles. Afterwards, there was a huge mass loss after 180 °C, which was caused by thermal decomposition of the organic matrix modified on the surface of the mesoporous silica particles. Ultimately, it was calculated that the content of thymol modified on MCM-41 and SBA-15 mesoporous nanoparticles was 3.41% and 5.82%. These data were used in the subsequent comparison of antibacterial tests with different contents of thymol.

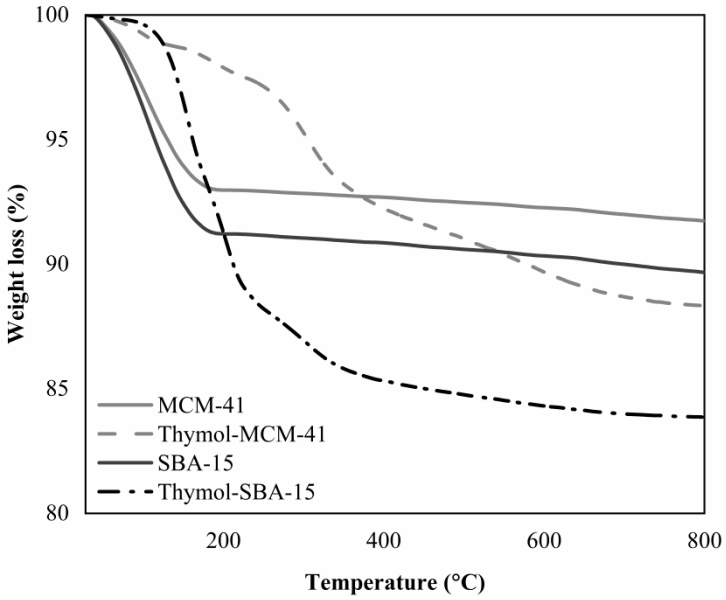

Figure 4. TGA curve of MCM-41, SBA-15, Thy-MCM-41, and Thy-SBA-15.

The porosity of mesoporous silica could be determined by analyzing N_2 adsorption/desorption isotherms of different mesoporous silica. As shown in Figure 5, considering the classification of the International Union of Pure and Applied Chemistry (IUPAC), all mesoporous silica particles exhibited a typical IV curve and had an h1 hysteresis loop, which meant that they had complete and regular mesoporous structure [31]. Moreover, the functionalized mesoporous silica nanoparticles had similar curves compared with the unmodified particles, which further demonstrated that the modified mesoporous silica particles still kept their unique ordered mesoporous structure.

As shown in Figure 6, the mesoporous structures and degree of order of different mesoporous silica nanoparticles were characterized by small-angle XRD. All samples showed three diffraction peaks corresponding to the (100), (110), and (200) atomic planes associated with two-dimensional cylindrical pores arranged in p6mm hexagonal symmetry [32]. By comparing the XRD curves of MCM-41, SBA-15, Thy-MCM-41, and Thy-SBA-15, it could be concluded that two diffraction curves were similar in shape, but the diffraction intensity of Thy-MCM-41 was slightly reduced and slightly shifted. The diffraction intensity of Thy-SBA-15 exhibited the same phenomenon as well. The main reason was that there were thymol groups in the holes of Thy-MCM-41 and Thy-SBA-15, which led to the reduction of the order of mesoporous holes. Therefore, this phenomenon proved the successful grafting of thymol [33]. Nevertheless, the main reflectance peak of the small-angle XRD pattern kept the original shape, indicating that the ordered mesoporous structure of the composites had not changed due to functionalization. The results were consistent with those of FESEM.

3.2. Antibacterial Activity of Functionalized Mesoporous Silicon

Using the growth inhibition rate of typical foodborne microorganisms, such as *E. coli* (Gram-negative) and *S. aureus* (Gram-positive), as the index, the antibacterial activities of free thymol, Thy-MCM-41, and Thy-SBA-15 were determined. Given the TGA results, the grafting rate of thymol on different carriers was obtained. The MBC of thymol grafted on the two carriers could be measured. MBC represented a 99.9% reduction in the growth of the initial inoculated bacteria, which equaled complete inhibition [34]. Figure 7 presents the growth reduction of *E. coli* and *S. aureus* treated with free thymol, Thy-MCM-41, and Thy-SBA-15 for 24 h. Generally, the larger the growth reduction was, the better the anti-bacterial activity would appear.

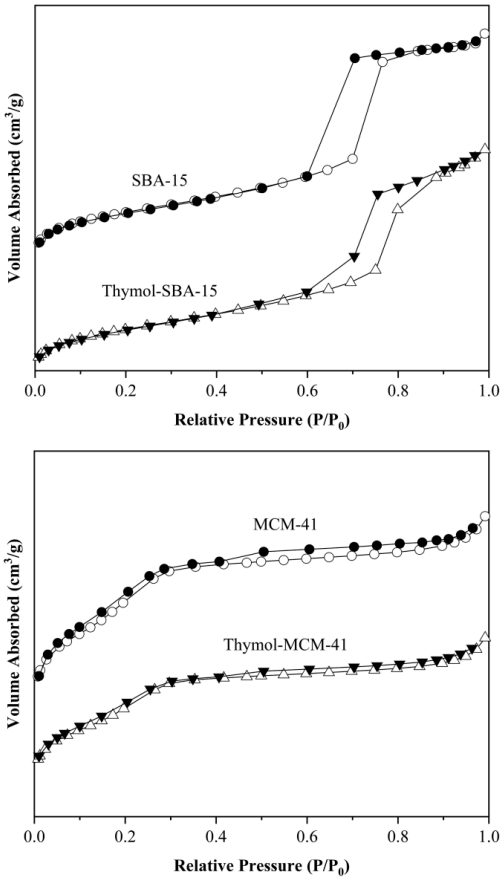

Figure 5. N_2 adsorption/desorption isotherms of MCM-41, SBA-15, Thy-MCM-41, and Thy-SBA-15.

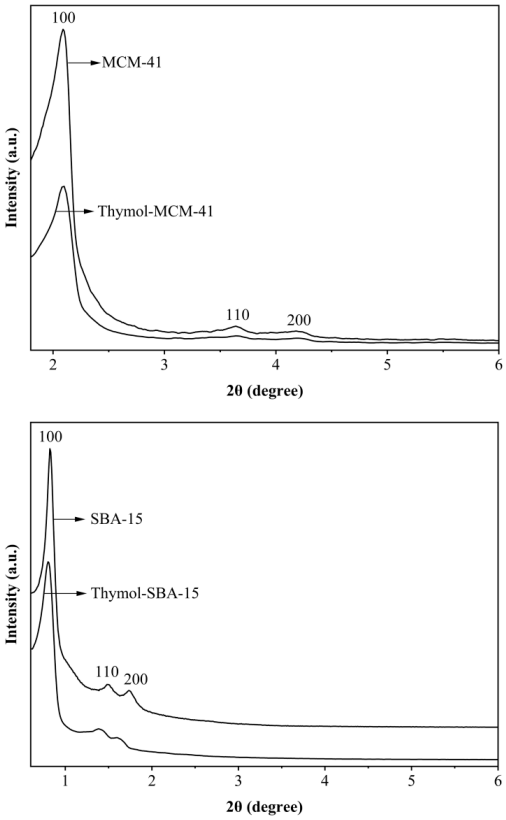

Figure 6. Small-angle XRD of MCM-41, SBA-15, Thy-MCM-41, and Thy-SBA-15.

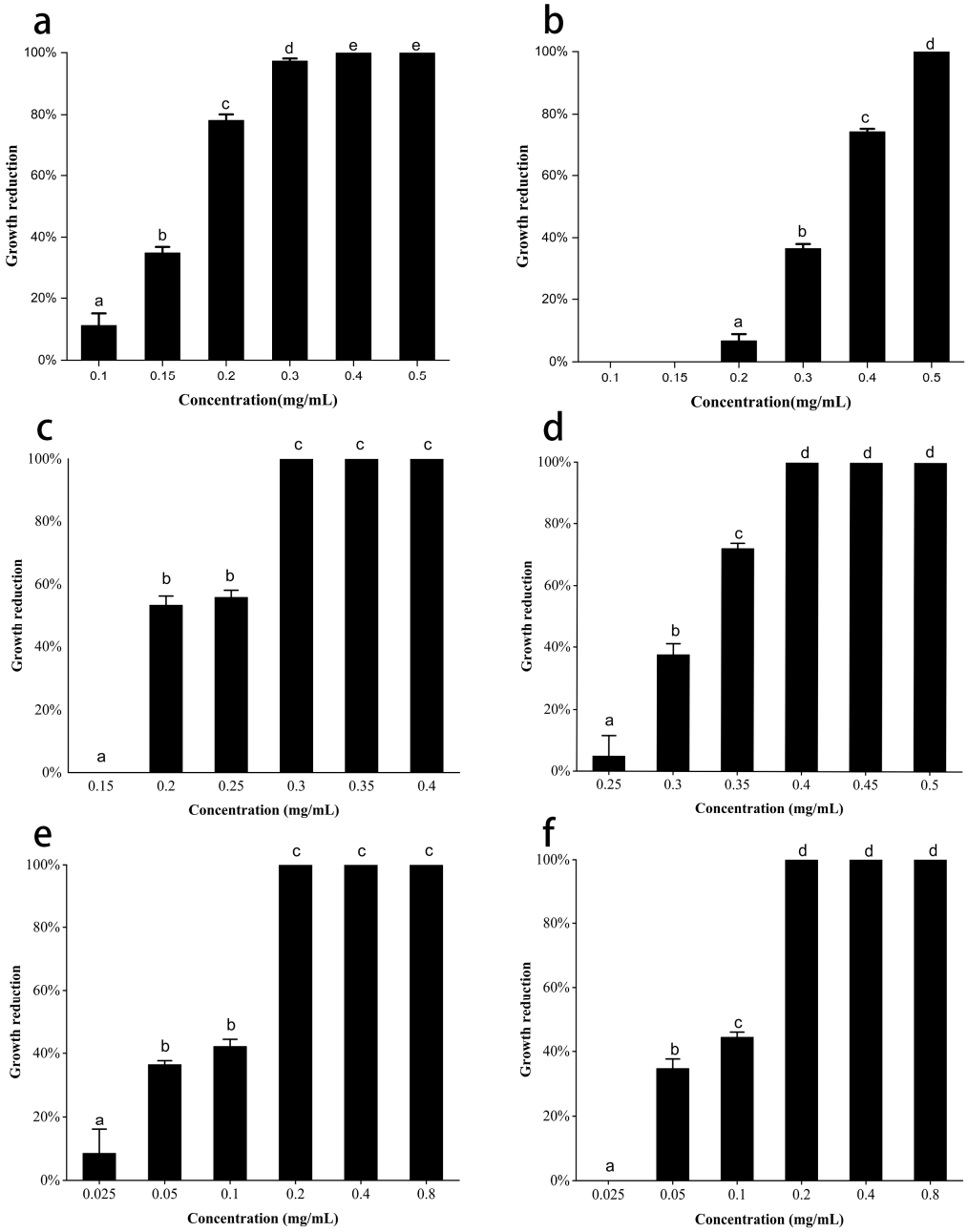

Figure 7. Growth reduction of *E. coli* and *S. aureus* treated with different concentrations of (**a**,**b**) free thymol; (**c**,**d**) Thy-MCM-41; and (**e**,**f**) Thy-SBA-15. The same letters in the bars show homogeneous group membership ($p < 0.05$).

The effect of free thymol on the growth of *E. coli* and *S. aureus* is shown in Figure 7a,b. The growth of *E. coli* was completely inhibited at a range from 0.4 mg mL^{-1} to 0.5 mg mL^{-1} and minor inhibition of *E. coli* was observed at concentrations between 0.1 mg mL^{-1} and 0.2 mg mL^{-1}. The MBC of free thymol against *E. coli* was at 0.4 mg mL^{-1}, which was similar to the previous studies [35]. Observing the inhibition of free thymol on the growth of *S. aureus*, it could be found that it did not inhibit the growth of *S. aureus* between 0.1–0.15 mg mL^{-1}, partially inhibited growth between 0.2-0.4 mg mL^{-1}, and reached complete inhibition at 0.5 mg mL^{-1}. The MBC for *S. aureus* at 0.5 mg mL^{-1}, which was consistent with the study of Rua, Fernandez-Alvarez [34]. These results suggest greater antimicrobial activity of thymol against Gram-negative bacteria, which is in accordance with the study of Gutiérrez-Larraínzar, Rúa [33]. The Gram-positive bacteria exhibiting

less susceptibility to antimicrobial components could be attributed to its outer membrane surrounding the cell wall, which restricts diffusion of hydrophobic compounds through its lipopolysaccharide covering.

As shown in Figure 7c, the MBC of Thy-MCM-41 against *E. coli* was 0.3 mg mL^{-1}. By observation, the effect of Thy-MCM-41 on the growth rate of *E. coli* could be divided into three stages. At the initial period, around 0.15 mg mL^{-1}, Thy-MCM-41 did not inhibit the growth rate of *E. coli* at all. Afterwards, Thy-MCM-41 could partially inhibit the growth of *E. coli* from 0.2 mg mL^{-1} to 0.25 mg mL^{-1}. Finally, the growth of *E. coli* was completely inhibited in the concentration range of 0.3-0.4 mg mL^{-1}. The MBC of Thy-MCM-41 against *E. coli* was at 0.3 mg mL^{-1}, which was slightly smaller than the MBC of free thymol. Similarly, the MBC of Thy-MCM-41 against *S. aureus* was 0.4 mg mL^{-1}, which was slightly lower than that of free thymol as well (Figure 7d). In the concentration range from 0.25 to 0.35 mg mL^{-1}, the growth inhibition rate of Thy-MCM-41 on *S. aureus* increased gradually, which was 4.84%, 37.60%, and 72.06%, respectively. The growth of *S. aureus* was completely inhibited in the range of 0.4–0.5 mg mL^{-1}.

In fact, the same trend could also be observed in the Thy-SBA-15 shown in Figure 7e,f. The inhibitory effect of Thy-SBA-15 on *E. coli* could be divided into partial inhibition and complete inhibition. The inhibitory effect on *E. coli* increased with the concentration, and the inhibition rate reached 37.30% and 42.13% at concentrations of 0.05 mg mL^{-1} and 0.1 mg mL^{-1}, respectively. Since the growth of *E. coli* was completely inhibited during the concentration range of 0.2–0.8 mg mL^{-1}, MBC of Thy-SBA-15 was 0.2 mg mL^{-1}. Obviously, Thy-SBA-15 also achieved complete inhibition against *S. aureus* in the concentration range of 0.2-0.8 mg mL^{-1}, namely the MBC was 0.2 mg mL^{-1}. In conclusion, the MBC of Thy-SBA-15 against *E. coli* and *S. aureus* was the same as Thy-SBA-15, which was lower than the free thymol. Studies have shown that the great antibacterial effect of immobilized molecules is due to the high surface concentration of anchored bioactive compounds in the surface of particles in direct contact with the cell membrane, which activates the membrane destruction mechanism [36,37].

In summary, these results indicated that functionalized silica carries enhanced antimicrobial activity of free thymol, which confirmed the success of the antibacterial strategy.

3.3. Antibacterial Mechanism

With the intention of further exploring the antibacterial mechanism of functionalized nanoparticles, the morphological changes of *E. coli* and *S. aureus* cells both before and after treatment with Thy-SBA-15 were observed by FESEM. As provided in Figure 8a, before treatment with Thy-SBA-15, *E. coli* cells were relatively smooth, with a complete cell membrane and cell wall. In contrast, the *E. coli* had rough and partially hollow cell surfaces after treatment, suggesting that the cell membrane was completely destroyed (Figure 8b). Similarly, *S. aureus* without Thy-SBA-15 treatment appeared to have the same status with *E. coli* (Figure 8c). Compared with the untreated control, *S. aureus* showed a rough surface and damaged cell walls after Thy-SBA-15 treatment (Figure 8d).

Apparently, this fact was related to the thymol grafted onto mesoporous silicon, which led to the destruction of cell walls and membranes in food-borne microbial cells [38,39].

The mechanism of thymol action has been reported in previous studies [11]. The phenolic hydroxyl group contained in thymol was the main functional group, which played an important role of bacteriostat [17,26]. Although thymol was covalently attached to silica nanomaterials, it still retained an effective antibacterial effect. Indeed, the germicidal mechanism of thymol might not have changed compared with previous reports. This may be due to the hydrophobicity of thymol, which can interact with lipids on the bacterial cell membrane, increasing the permeability of the cell membrane, resulting in cell leakage and affecting bacterial activity. Secondly, thymol might also interact with membrane proteins and intracellular targets, which impede the repair of damaged membranes.

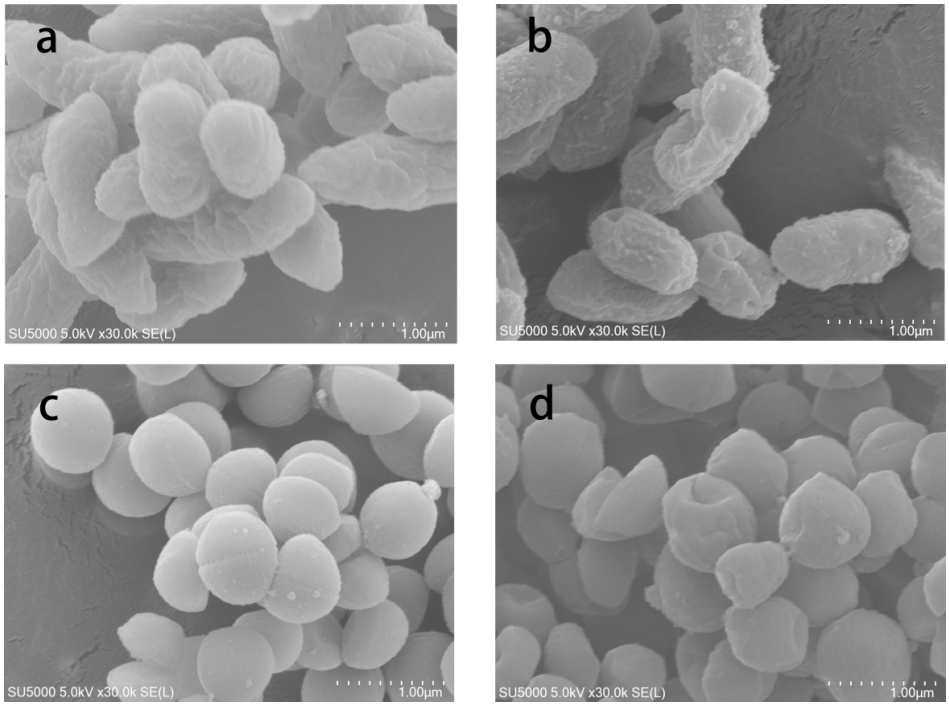

Figure 8. FESEM images of *E. coli* and *S. aureus* (**a**,**c**) untreated and (**b**,**d**) after functionalized SBA-15 treatment.

4. Conclusions

In summary, we presented a post-grafting method to immobilize thymol on mesoporous silica nanomaterials, aimed at preparing a new efficient antibacterial system. This immobilized thymol method effectively improves the stability and antibacterial activity of free thymol. Given the result of characterization, it was found that the functionalization process did not change the specific morphology and ordered pore structure of the mesoporous material. More encouragingly, both functionalized SBA-15 and MCM-41 showed higher bactericidal efficiency, effectively killing both pathogenic microorganisms. Therefore, nanoparticles immobilized by essential oils have great potential for food industry applications.

Author Contributions: Conceptualization, T.N. and S.W.; methodology, L.W.; software, L.W.; validation, T.N. and S.W.; formal analysis, L.W.; investigation, L.W.; resources, T.N. and S.W.; writing—original draft preparation, L.W.; writing—review and editing, L.W.; visualization, T.N. and S.W.; supervision, T.N. and S.W.; project administration, T.N. and S.W.; funding acquisition, T.N. and S.W. All authors have read and agreed to the published version of the manuscript.

Funding: This research received no external funding.

Institutional Review Board Statement: Not applicable.

Informed Consent Statement: Not applicable.

Data Availability Statement: The data presented in this study are available on request from the corresponding author.

Conflicts of Interest: The authors declare no conflict of interest.

References

1. Roca, I.; Akova, M.; Baquero, F.; Carlet, J.; Cavaleri, M.; Coenen, S.; Cohen, J.; Findlay, D.; Gyssens, I.; Heuer, O.E.; et al. Corrigendum to "The global threat of antimicrobial resistance: Science for intervention" [New Microbes New Infect 6 (2015): 22–29]. *New Microbes New Infect* **2015**, *8*, 175. [CrossRef] [PubMed]
2. Havelaar, A.H.; Kirk, M.D.; Torgerson, P.R.; Gibb, H.J.; Hald, T.; Lake, R.J.; Praet, N.; Bellinger, D.C.; de Silva, N.R.; Gargouri, N.; et al. World Health Organization Global Estimates and Regional Comparisons of the Burden of Foodborne Disease in 2010. *PLoS Med.* **2015**, *12*, e1001923. [CrossRef] [PubMed]

3. Burt, S. Essential oils: Their antibacterial properties and potential applications in foods—A review. *Int. J. Food Microbiol.* **2004**, *94*, 223–253. [CrossRef] [PubMed]
4. Capeletti, L.B.; de Oliveira, L.F.; Goncalves, K.d.A.; Affonso de Oiveira, J.F.; Saito, A.; Kobarg, J.; Zimnoch dos Santos, J.H.; Cardoso, M.B. Tailored Silica-Antibiotic Nanoparticles: Overcoming Bacterial Resistance with Low Cytotoxicity. *Langmuir* **2014**, *30*, 7456–7464. [CrossRef]
5. Bernardos, A.; Marina, T.; Zacek, P.; Perez-Esteve, E.; Martinez-Manez, R.; Lhotka, M.; Kourimska, L.; Pulkrabek, J.; Kloucek, P. Antifungal effect of essential oil components against Aspergillus niger when loaded into silica mesoporous supports. *J. Sci. Food Agric.* **2015**, *95*, 2824–2831. [CrossRef]
6. Gyawali, R.; Ibrahim, S.A. Natural products as antimicrobial agents. *Food Control* **2014**, *46*, 412–429. [CrossRef]
7. Allahverdiyev, A.M.; Kon, K.V.; Abamor, E.S.; Bagirova, M.; Rafailovich, M. Coping with antibiotic resistance: Combining nanoparticles with antibiotics and other antimicrobial agents. *Expert Rev. Anti-Infect. Ther.* **2011**, *9*, 1035–1052. [CrossRef]
8. Rai, M.; Paralikar, P.; Jogee, P.; Agarkar, G.; Ingle, A.P.; Derita, M.; Zacchino, S. Synergistic antimicrobial potential of essential oils in combination with nanoparticles: Emerging trends and future perspectives. *Int. J. Pharm.* **2017**, *519*, 67–78. [CrossRef]
9. Nazzaro, F.; Fratianni, F.; De Martino, L.; Coppola, R.; De Feo, V. Effect of essential oils on pathogenic bacteria. *Pharmaceuticals* **2013**, *6*, 1451–1474. [CrossRef]
10. Ruiz-Rico, M.; Perez-Esteve, E.; Bernardos, A.; Sancenon, F.; Martinez-Manez, R.; Marcos, M.D.; Barat, J.M. Enhanced antimicrobial activity of essential oil components immobilized on silica particles. *Food Chem.* **2017**, *233*, 228–236. [CrossRef]
11. Ultee, A.; Bennik, M.H.; Moezelaar, R. The phenolic hydroxyl group of carvacrol is essential for action against the food-borne pathogen Bacillus cereus. *Appl. Environ. Microbiol.* **2002**, *68*, 1561–1568. [CrossRef] [PubMed]
12. Lv, F.; Liang, H.; Yuan, Q.; Li, C. In vitro antimicrobial effects and mechanism of action of selected plant essential oil combinations against four food-related microorganisms. *Food Res. Int.* **2011**, *44*, 3057–3064. [CrossRef]
13. Turek, C.; Stintzing, F.C. Stability of Essential Oils: A Review. *Compr. Rev. Food Sci. Food Saf.* **2013**, *12*, 40–53. [CrossRef]
14. Bravo Cadena, M.; Preston, G.M.; Van der Hoorn, R.A.L.; Townley, H.E.; Thompson, I.P. Species-specific antimicrobial activity of essential oils and enhancement by encapsulation in mesoporous silica nanoparticles. *Ind. Crops Prod.* **2018**, *122*, 582–590. [CrossRef]
15. Ribes, S.; Ruiz-Rico, M.; Pérez-Esteve, É.; Fuentes, A.; Barat, J.M. Enhancing the antimicrobial activity of eugenol, carvacrol and vanillin immobilised on silica supports against Escherichia coli or Zygosaccharomyces rouxii in fruit juices by their binary combinations. *LWT* **2019**, *113*, 108326. [CrossRef]
16. Ribes, S.; Ruiz-Rico, M.; Pérez-Esteve, É.; Fuentes, A.; Talens, P.; Martínez-Máñez, R.; Barat, J.M. Eugenol and thymol immobilised on mesoporous silica-based material as an innovative antifungal system: Application in strawberry jam. *Food Control* **2017**, *81*, 181–188. [CrossRef]
17. García-Ríos, E.; Ruiz-Rico, M.; Guillamón, J.M.; Pérez-Esteve, É.; Barat, J.M. Improved antimicrobial activity of immobilised essential oil components against representative spoilage wine microorganisms. *Food Control* **2018**, *94*, 177–186. [CrossRef]
18. Li, W.; Liu, J.; Zhao, D. Mesoporous materials for energy conversion and storage devices. *Nat. Rev. Mater.* **2016**, *1*, 16023. [CrossRef]
19. Llopis-Lorente, A.; Lozano-Torres, B.; Bernardos, A.; Martinez-Manez, R.; Sancenon, F. Mesoporous silica materials for controlled delivery based on enzymes. *J. Mater. Chem. B* **2017**, *5*, 3069–3083. [CrossRef]
20. Hou, J.; Weng, R.; Jiang, W.; Sun, H.; Xia, J.; Liu, Y.; Sheng, J.; Song, Y. In-situ preparation of novel sedimentary rock-like Fe3O4 by rice-husk mesoporous silica as templates for effective remove As(III) from aqueous solutions. *J. Environ. Chem. Eng.* **2021**, *9*, 105866. [CrossRef]
21. Calvo, A.; Joselevich, M.; Soler-Illia, G.J.A.A.; Williams, F.J. Chemical reactivity of amino-functionalized mesoporous silica thin films obtained by co-condensation and post-grafting routes. *Microporous Mesoporous Mater.* **2009**, *121*, 67–72. [CrossRef]
22. Wen, H.; Zhou, X.; Shen, Z.; Peng, Z.; Chen, H.; Hao, L.; Zhou, H. Synthesis of ZnO nanoparticles supported on mesoporous SBA-15 with coordination effect-assist for anti-bacterial assessment. *Colloids Surf. B Biointerfaces* **2019**, *181*, 285–294. [CrossRef] [PubMed]
23. Moghadam, H.D.; Sani, A.M.; Sangatash, M.M. Inhibitory Effect ofHelichrysum arenariumEssential Oil on the Growth of Food Contaminated Microorganisms. *J. Essent. Oil Bear. Plants* **2014**, *17*, 911–921. [CrossRef]
24. Park, S.-Y.; Barton, M.; Pendleton, P. Mesoporous silica as a natural antimicrobial carrier. *Colloids Surf. A Physicochem. Eng. Asp.* **2011**, *385*, 256–261. [CrossRef]
25. Fuentes, C.; Ruiz-Rico, M.; Fuentes, A.; Ruiz, M.J.; Barat, J.M. Degradation of silica particles functionalised with essential oil components under simulated physiological conditions. *J. Hazard. Mater.* **2020**, *399*, 123120. [CrossRef] [PubMed]
26. Gholamzadeh, P.; Mohammadi Ziarani, G.; Zandi, F.; Abolhasani Soorki, A.; Badiei, A.; Yazdian, F. Modification of fumed silica surface with different sulfonamides via a postsynthesis method and their application as antibacterial agents. *Comptes Rendus Chim.* **2017**, *20*, 833–840. [CrossRef]
27. Gamez, E.; Elizondo-Castillo, H.; Tascon, J.; Garcia-Salinas, S.; Navascues, N.; Mendoza, G.; Arruebo, M.; Irusta, S. Antibacterial Effect of Thymol Loaded SBA-15 Nanorods Incorporated in PCL Electrospun Fibers. *Nanomaterials* **2020**, *10*, 616. [CrossRef]
28. Marinescu, G.; Culita, D.C.; Romanitan, C.; Somacescu, S.; Ene, C.D.; Marinescu, V.; Negreanu, D.G.; Maxim, C.; Popa, M.; Marutescu, L.; et al. Novel hybrid materials based on heteroleptic Ru(III) complexes immobilized on SBA-15 mesoporous silica as highly potent antimicrobial and cytotoxic agents. *Appl. Surf. Sci.* **2020**, *520*, 146379. [CrossRef]

29. Gonzalez, B.; Colilla, M.; Diez, J.; Pedraza, D.; Guembe, M.; Izquierdo-Barba, I.; Vallet-Regi, M. Mesoporous silica nanoparticles decorated with polycationic dendrimers for infection treatment. *Acta Biomater.* **2018**, *68*, 261–271. [CrossRef]
30. Gao, F.; Zhou, H.; Shen, Z.; Zhu, G.; Hao, L.; Chen, H.; Xu, H.; Zhou, X. Long-lasting anti-bacterial activity and bacteriostatic mechanism of tea tree oil adsorbed on the amino-functionalized mesoporous silica-coated by PAA. *Colloids Surf. B Biointerfaces* **2020**, *188*, 110784. [CrossRef]
31. Ruiz-Rico, M.; Fuentes, C.; Pérez-Esteve, É.; Jiménez-Belenguer, A.I.; Quiles, A.; Marcos, M.D.; Martínez-Máñez, R.; Barat, J.M. Bactericidal activity of caprylic acid entrapped in mesoporous silica nanoparticles. *Food Control* **2015**, *56*, 77–85. [CrossRef]
32. Hamoud, R.; Zimmermann, S.; Reichling, J.; Wink, M. Synergistic interactions in two-drug and three-drug combinations (thymol, EDTA and vancomycin) against multi drug resistant bacteria including E. coli. *Phytomedicine* **2014**, *21*, 443–447. [CrossRef] [PubMed]
33. Gutiérrez-Larraínzar, M.; Rúa, J.; Caro, I.; de Castro, C.; de Arriaga, D.; García-Armesto, M.R.; del Valle, P. Evaluation of antimicrobial and antioxidant activities of natural phenolic compounds against foodborne pathogens and spoilage bacteria. *Food Control* **2012**, *26*, 555–563. [CrossRef]
34. Rua, J.; Fernandez-Alvarez, L.; de Castro, C.; del Valle, P.; de Arriaga, D.; Rosario Garcia-Armesto, M. Antibacterial Activity Against Foodborne Staphylococcus aureus and Antioxidant Capacity of Various Pure Phenolic Compounds. *Foodborne Pathog. Dis.* **2011**, *8*, 149–157. [CrossRef] [PubMed]
35. Boye, A.; Addo, J.K.; Acheampong, D.O.; Thomford, A.K.; Asante, E.; Amoaning, R.E.; Kuma, D.N. The hydroxyl moiety on carbon one (C1) in the monoterpene nucleus of thymol is indispensable for anti-bacterial effect of thymol. *Heliyon* **2020**, *6*, e03492. [CrossRef] [PubMed]
36. Di Pasqua, R.; Mamone, G.; Ferranti, P.; Ercolini, D.; Mauriello, G. Changes in the proteome of Salmonella enterica serovar Thompson as stress adaptation to sublethal concentrations of thymol. *Proteomics* **2010**, *10*, 1040–1049. [CrossRef] [PubMed]
37. Hartl, F.U.; Bracher, A.; Hayer-Hartl, M. Molecular chaperones in protein folding and proteostasis. *Nature* **2011**, *475*, 324–332. [CrossRef] [PubMed]
38. Li, Y.; Shao, X.; Xu, J.; Wei, Y.; Xu, F.; Wang, H. Tea tree oil exhibits antifungal activity against Botrytis cinerea by affecting mitochondria. *Food Chem.* **2017**, *234*, 62–67. [CrossRef]
39. Marchese, A.; Orhan, I.E.; Daglia, M.; Barbieri, R.; Di Lorenzo, A.; Nabavi, S.F.; Gortzi, O.; Izadi, M.; Nabavi, S.M. Antibacterial and antifungal activities of thymol: A brief review of the literature. *Food Chem.* **2016**, *210*, 402–414. [CrossRef]